The Ability of Red Mangrove, Gray Mangrove, and Mangrove Palm to Reduce Erosion Rate at The Northern Coast of Bengkalis Island Indonesia

Noerdin Basir[1], Tetsuya Hiraishi[2], Zev Al Jauhari[3]

{noerbas@gmail.com[1], hiraishi.tetsuya.2c@kyoto-u.ac.jp[2], zevaljauhari@polbeng.ac.id [3]}

Department of Civil Engineering, Bengkalis State Polytechnic, Sungai Alam, Bengkalis, 28711, Indonesia[1,3]

Ujigawa Open Laboratory, Yoko-Oji, Shimomisu Fushimi-Ku, Address, Kyoto, 612-8242, Japan[2]

Abstract. Bengkalis Island has been experiencing a severe coastal erosion process, particularly on the northern coast. In 1955, the north shore of Bengkalis Island was protected by mangrove forest, which has a function as a natural barrier against coastal erosion. Currently, the condition of this area has been severely eroded due to the human activity of mangrove deforest. The coastal morphology of Bengkalis is a peatland and known as Bog Burst. Almost 70% erosion type that happens in Bengkalis Island are toppling failure and sliding failure, the effect of tidal wave oscillation promoted the formation and widening of tension cracks, parallel to the bank edge, the presence of tension cracks led to an unstable bank configuration, triggering mass failure, the tensile strength of the soil, so erosion occurs. Three types of mangroves that are often encountered in the northern coast of the Bengkalis island are namely red mangrove, grey mangrove and palm mangrove. This research aims to study the erosion process and the ability of all three types of mangroves in reducing the erosion rate at Bengkalis island from a numerical approach. Xbeach 1D model will be employed to simulate the wave attenuation in the mangrove tree and calculate the vegetation effect to reduce the erosion rate. The numerical model is based on the Mendez and Lozada (2004), which is using the vegetation stem width and density to calculate the vegetation drag force on the water column for wave energy loss. The mangrove tree will be defined by multiple height segments of the species with different properties, the value is given from the bottom to the top. The simulation results show that the mangrove palm, although only defined has 2 layers, namely the stem and canopy but overall have a better ability to reduce the erosion rate.

Keywords: Erosion rates, tropical coast, mangrove, x-beach.

1 Introduction

In 1955, the north shore of Bengkalis Island was protected by mangrove forest, which has a function as a natural barrier against coastal erosion. Currently, the condition of the area has been severely eroded due to the human activity of mangrove deforest. The coastal morphology of

ABEC 2023, September 21, Bengkalis, Indonesia

DOI 10.4108/eai.21-9-2023.2342878

Bengkalis is a peatland and known as Bog Burst. Mass failure is episodic changes in the morphology of banks or cliffs in rivers, estuary, or coasts [1]. When included in the toppling model, the effect of vegetation may result in a delay of the mass failure, but a more detailed description of the root mat structure; and the soil stress characteristic would be needed. It is important to stress that the toppling failure model [2] describes three types of erosion failure, which is the overhanging block of soil that occurs once the scour at the bank toe exceeds a limiting value, as seen in Figure 1.

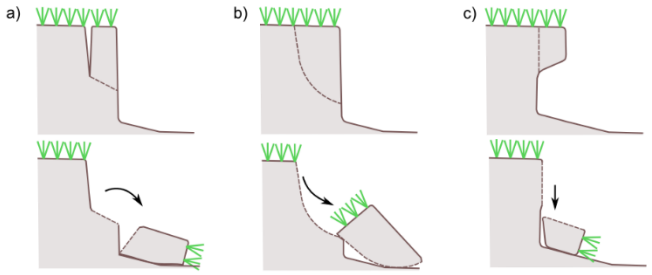

Fig. 1. Mass failure modes of Bengkalis banks a) Toppling failure, b) Rotational sliding, c) Cantiliver failure [3]

The failure process is assumed to occur instantaneously once a specific threshold of stress is exceeded. However, the inclusion of the vegetation would require a progressive failure mechanism, due to the progressive detachment of the block of soil from the failure surface induced by the cumulative effect of waves. Indeed, even if the extension failure surface would be progressively reduced by the effect of waves, the root mat may continue to offer a resistance against the mass failure. Furthermore, different typologies of plants may diversely affect the failure process since the extent of the root mat can have a control on the depth of the formation of tension cracks and, as a consequence, on the dimensions of the block subject to failure.

Mentayan Beach is located in the northern part of the Bengkalis Island. For Mentayan people, erosion is a scary thing, especially for those living in coastal areas that are directly facing the Straits of Malacca, which is famous for large tidal waves that trigger the abrasion rate. Hundreds of meters of gardens and agricultural land, even the resident homes are threatened to collapse every year.

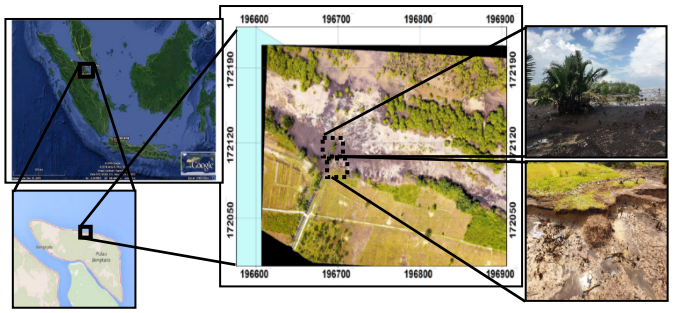

Fig. 2. Research area

Figure 2 shows the location of the research area. The local government of Bengkalis Regency through the environmental Department and MAP's a local NGO partners Yayasan Laksamana Samudra, in partnership with CRM project called Co-Fish established 10 mangrove stewardship groups that have made efforts to replant mangrove trees. They chose the grey mangrove or known as Avicennia Marina as the kind of mangrove to be planted because it can be growing in tropical areas and one of the most tolerant of mangroves to salinity and aridity, also it can be growth rapidly.

The main objective of this research is to investigate the erosion process and the ability of the red mangrove, gray mangrove, and mangrove palm in reducing the erosion rate from a numerical approach.

2 Research Methods

2.1 Field Survey and Data Measurement

The measurement campaigns base on geo-informatics activity composed of both terrestrial survey and photogrammetry to produce the bathymetry data and high-resolution image for the interest area. All of the images from the photogrammetry result need to be geo-referenced (see Table 1) by the ground control point to get a better result.

Table 1. Geo-reference result of Selatbaru Beach

ID	X source	Y source	X map	Y map	Rms err
1	196600,3	172153,9	196600,6	172152,6	0,066
2	196535,2	172145,6	196536,1	172142,9	-0,033
3	196557,9	172272,8	196556,3	172267,8	-0,016
4	196665,8	172284,2	196663,1	172279,7	0,020
5	196714	172180	196712,7	172177,5	-0,036
Total RMS error					0,450

The coordinate system of WGS 84 is used. We could see the Total RMS error less than 1, which means the Georeference calculation accepted.

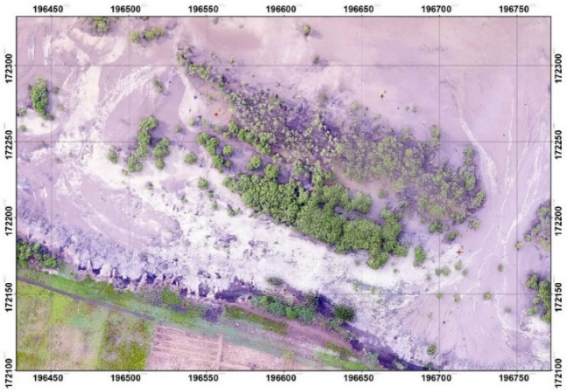

Fig. 3. Map which had been rectified

Three data loggers are installed at two different locations, pt.2 and pt.3 data loggers, are installed at the offshore side with a distance of 5 m away from the mangrove area, while loggers number two, pt.1, are installed on onshore, 5 m after the mangrove areas. The data logger records at 1-second intervals. The data from all loggers will be used as validation for the wave reduction factor and current velocity for the x-beach numerical model.

Table 2. Location of the logger

ID	X source	Y source	X map	Y map	Rms err
1	196600,3	172153,9	196600,6	172152,6	0,066
2	196535,2	172145,6	196536,1	172142,9	-0,033
3	196557,9	172272,8	196556,3	172267,8	-0,016

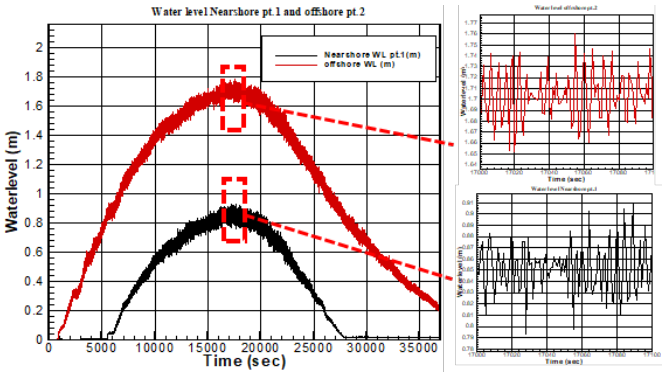

Fig. 4. Water level recorded by hobo logger black line indicated onshore side and red line offshore side (left), detail of wave high for every stations (right)

The maximum high tidal is 2.51 m, and the minimum low tidal is 0.78 m. There is a 1.73 m difference between high and low tidals. Base on the condition of the research area, water only floods and touches the cliffs during high tides. The met-ocean data records by wave logger at an approximate water depth of 0 to 2 m. The wave data logger recorded every 1 second. A significant wave occurs at 0.57 m height and 6 second period.

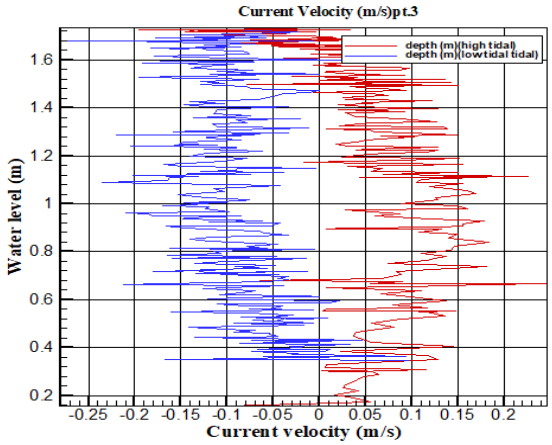

Fig. 5. Current velocity recorded by ADCP pt.3; red and blue lines indicated current velocity in vertical layer in high and low tidal conditions, respectively

2.2 Modelling Approach

The role played by vegetation in the mass failure processes is still an open issue. On one hand, vegetation can increase the porosity of the soil and the filtration velocity, possibly reducing soil resistance; on the other hand, the presence of the root mat can induce an additional cohesion to the soil matrix reducing the depth of the cracks and their frequency of occurrence [4]. Vegetation can delay the failure of the vegetated clods [5]. The phenomenon of toppling failure that occurs can be explained through cross-sectional of the shorelines in x-y view.

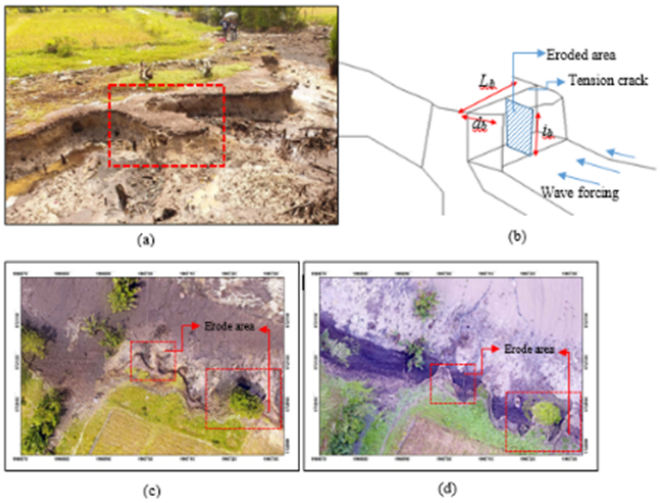

Fig. 6. (a) Unstable bank configuration of Mentayan Beach, (b) Sketch representing an unstable bank configuration, (c) Aerial images taken 19 March 2019, (d) Aerial images taken 22 May 2019

From the figure, it can be seen that there has been an erosion in the area marked with a rectangle during observation starting from 19 March 2019 to 22 May 2019, during the erosion period

occurred just behind the mangrove area, if observed in the picture (d) there is a mangrove tree at the edge of the shoreline that protects the cliff behind it to avoid erosion. To explain the phenomenon, the modeling approach as shown in figure (b) using the modeled system behaves dynamically as a consequence of the external forces. The failure surface is located at a depth from the top of the bank equal to the depth of the tension crack i_b, with the dimensions are assumed equal to the width L_b and length d_b of the block. The block mass can be calculated as:

$$m_b = \rho_s \cdot d_b \cdot i_b \cdot L_b \tag{1}$$

When the waves act on the block, it is partially free to oscillate due to the soil at the base and the possible presence of water inside the crack [6]. The hydrodynamic mass for rotation motions, regarding to the base of the block, is estimated through [7]:

$$m_{hr} = 0{,}218.\rho.L_b \cdot Z^2 \tag{2}$$

With Z is the elevation of the rotating point, which is at the point of $d_b/2$, the moment of inertia I_b can calculate as:

$$I_b = m_b \cdot \left(\frac{i_b^2 + d_b^2}{12} \right) + \left(m_b + m_{hr}\right) \left(\frac{i_b^2}{4} \right) \tag{3}$$

Different erosion behavior occurs along the coastline depending on the morphological conditions and tidal conditions, to illustrate the condition of the coastline retreat due to Toppling failure, a simple mathematical model is described as follows.

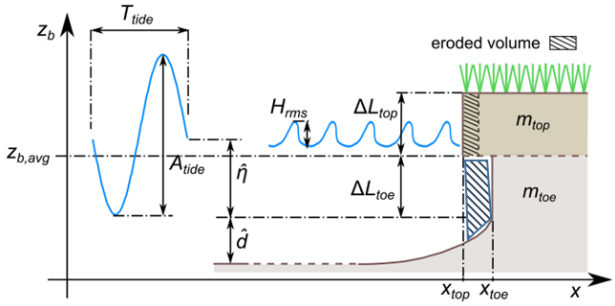

Fig. 7. Sketch of the bank retreat model due to cantilever failures (bendoni 2016)

The upper part is eroded when the water surface elevation to the toe of the bank ñ falls between $Z_{b,avg}$ and $Z_{b,avg} + \Delta L_{top}$, whereas the lower part is eroded when the waterfall between $Z_{b,avg} - \Delta L_{top}$. The cumulative retreats of the two portions of the bank are calculated as:

$$x_{top}(t + \Delta t) = x_{top}(t) + \frac{m_{top} W}{\Delta L_{top}} \Delta_t \tag{4}$$

$$x_{toe}(t + \Delta t) = x_{toe}(t) + \frac{m_{toe} W}{\Delta L_{toe}} \Delta_t \tag{5}$$

In tidal environments sand (0:063 < d < 2 mm), silt (0:004 < d < 0:063 mm) and clay (d < 0:004 mm) are present in variable fractions. The ratio between clay and silt is fairly constant in these

environments [8], in this study very fine sediments are considered for the sand d_{50} = 0.2 mm for both Erosion rates for sand and mud can be calculated as:

$$E_m = \begin{cases} p_m E_m^*, & if\ p_m \geq p_{m,cr} \\ p_m E_s^*, & if\ p_m < p_{m,cr} \end{cases} \quad (6)$$

$$E_s = \begin{cases} (1-p_m) E_m^*, & if\ p_m \geq p_{m,cr} \\ (1-p_m) E_s^*, & if\ p_m < p_{m,cr} \end{cases} \quad (7)$$

Where E^*_m and E^*_s are the absolute volumetric erosion rates per unit area for the cohesive and non-cohesive regimes, respectively. The absolute erosion rate in the cohesive regime is:

$$E_m^* = \frac{1}{\rho_s} M_c \left(\frac{\tau_b}{\tau_{cr,c}} - 1 \right) H_f \left(\frac{\tau_b}{\tau_{cr,c}} - 1 \right) \quad (8)$$

In which M_c is the erosion parameter in the cohesive regime, $\tau_{cr,c}$ is the bottom shear stress, is the critical shear stress in the cohesive regime, and H_f is the Heaviside function. Similarly, the absolute erosion rate in the non-cohesive regime reads:

$$E_s^* = \frac{1}{\rho_s} M_{nc} T_{nc}^{\alpha_{nc}} \quad (9)$$

Where M_{nc} is the erosion parameter for the non-cohesive regime and T_{nc} a dimensionless transport parameter [9]:

$$T_{nc} = \left(\frac{\tau b}{\tau_{cr,c}} - 1 \right) H_f \left(\frac{\tau b}{\tau_{cr,c}} - 1 \right) \quad (10)$$

With the $\tau_{cr,c}$ critical shear stress in the non-cohesive regime. The values of the erosion parameter calculate as:

$$M_{nc} = \rho_s w_{s,s} F_s 0{,}015 \frac{d_{50,s}}{\alpha_s d_*^{0,3}} \quad (11)$$

$$M_c = \left(\frac{M_{nc}}{M_m} \right)^{\frac{1-p_m}{1-p_{m,cr}}} M_m \quad (12)$$

in which $\omega_{s,s}$ is the sand settling velocity, F_s is a shape factor accounting for the sediment distribution along the water column [9], α_c is the reference height from the bed for the sediment equilibrium concentration, d_* is the dimensionless grain size and M_m is the erosion parameter for pure mud, ranging from 10-5 to 10-3 kg/m^{2}s [10].

2.3 Wave dissipation by vegetation

In Xbeach is simplicity based on a wave orbital velocity calculated from linear wave theory, three short wave dissipation processes can be accounted for: wave breaking (D_w), bottom friction (D_f), and vegetation (D_w). The vegetation can be schematized in the number of vertical elements with each specific property. In this way, the damping effect of vegetation such as mangrove trees, with a relatively dense root system but sparse stem area, can be model. The dissipation term is then computed as the sum of the dissipation per vegetation layer.

$$D_v = \sum_{i=1}^{n_v} D_{v,i} \tag{13}$$

Where $D_{v,i}$ is the dissipation by vegetation in vegetation layer i and N_v is the number of vegetation layers. The dissipation per layer is given by

$$D_{v,i} = A_v \frac{\rho C_{d,i}, b_{v,i}, N_{v,i}}{2\sqrt{\pi}} \left(\frac{kg}{2\sigma} \right)^{(3)} H_{rms}^3 \tag{14}$$

$$A_v = \frac{(\sin h^3 k\alpha_1 h - \sin h^3 k\alpha_{i-1} h) + 3(\sin h.k\alpha_1 h - \sin h.k\alpha_{i-1} h)}{3k \cos h^3 kh} \tag{15}$$

Where $C_{d,i}$ is a drag coefficient, $b_{v,i}$ is the vegetation stem diameter $N_{v,i}$ is the vegetation density α_i is the relative vegetation height ($\frac{h_v}{h}$) for layer i.

Red mangroves or Rhizophora mangle can be distinguished by their long prop roots. It generally lives in intertidal zones which are inundated daily by the ocean. They exhibit some adaptations to this environment, including pneumatophores that elevate the plants above the water and allow them to respire oxygen even while their lower roots are submerged, the gray mangrove or known as Avicennia marina, is a species of mangrove tree classified in the plant family of Acanthaceae. As with other mangroves, it occurs in the intertidal zones of estuarine areas. Because of its ability to grow quickly, this type of mangrove becomes one of the choices for local governments in efforts to prevent erosion, this can be seen in the research location where most of the mangrove plants on the Mentayan coast planted by the local government are Avicennia marina. The mangrove palm or known as Nipah is a kind of palm that grows in the environment of mangroves forest or tidal areas near shorelines. These species best adapted to grow in areas with moderate only salt load, and circumscribing quite well the actual areas of occurrence of this palm tree in the gradient from seawater habitats to inland sites [11], and usually it growth behind a mangrove tree. Nipah tree trunks spread on the ground, forming rhizomes submerged by mud. Only the rosette leaves appear on the ground, so the Nipah looks as if it is not trunked. The fiber roots can reach 13 meters in length, and function as a barrier for the sediment deposit.

Fig. 8. Red mangrove (left), grey mangrove (middle), mangrove palm (right)

Vegetation plays a very important role in the process of mass failure. loss of vegetation may increase soil porosity and filtration speed, possibly reducing soil resistance. When included in the collision model, the effect of vegetation can cause a delay in mass failure. It is important to emphasize that in the collision failure model, the failure process is assumed to occur instantly once a certain stress threshold is exceeded. inclusion of vegetation will be able to reduce the wave energy from collisions of the cumulative effects of waves. Different plant typologies can affect the failure process because the extent of the root mate can have control of the wave height inhibition.

With the intention of to getting better results from numerical calculations, a vertical variation of mangrove trees, made by giving more than three layers. The main part of mangrove trees is roots, stem, and canopy. The species property will be defined by multiple height segments of the species with different properties, the value given from bottom to the top as seen in Figure 9.

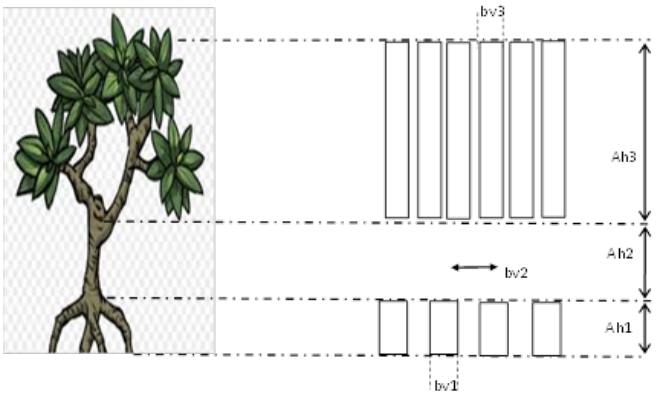

Fig. 9. Mangrove (left), the method of vertical layer from X-beach model (right)

Ah_1 is the height of root segment from bed level, Ah_2 defines as stem height and Ah_3 is the canopy height, bv1 is root diameter, bv_2 stem diameter, and bv_3 is canopy diameter. A high tree has a large diameter to maintain its stability, for mangrove density (N_1, N_2, N_3). The physical value of vegetation will be given in Table 1.

Table 3. Value of phisycal parameter of type 1 (api-api) and type 2 (bakau)

Vegeta-tion	Ah_1 (m)	Ah_2 (m)	Ah_3 (m)	bv_1 (m)	bv_2 (m)	bv_3 (m)	N_1 m^{-2}	N_2 m^{-2}	N_3 m^{-2}
Type 1 red	0,9	1,2	3,6	0,05	0,15	0,03	70	4	100
Type 2 grey	0,4	1,3	5	0,12	0,35	0,2	6	1	8
Type 2 palm	-	0,3	3,5	-	1	0,3	0,3	1	30

2.4 Wave Input

An X-Beach model is generally forced by waves on its offshore boundary. The detail of the wave motion within the model is described by the wave numeric in terms of the wave actions balance. JONSWAP wave spectrum input is used.

Table 4. JONSWAP Input Parameter

ID	Hrm0 (m)	Trep (sec)	WL (m)
Case 1	0,8	6	1,3
Case 2	1,1	6	1,3
Case 3	1,4	6	1,3
Case 4	0,8	8	1,3
Case 5	1,1	8	1,3
Case 6	1,4	8	1,3

The cross-shore profile came from the intended initial cross-shore profile in Mentayan Beach, as seen in cross A-A' at Figure 3. The cross profile is defined by the coordinates of x and y. The initial profile is shown by the solid red line, while the position of the mangrove plant is located between 100 m to 225 m; the grid spacing is 1 m with a total grid in the x- direction of 267.

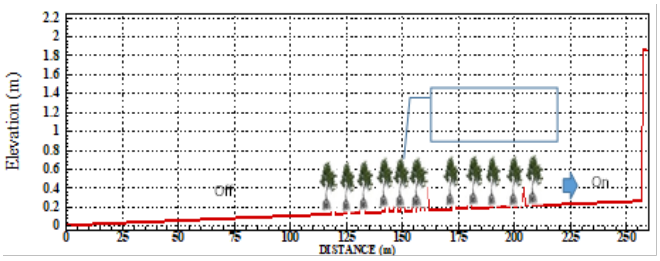

Fig. 10. Cross section profile. A-A'

2.5 Model Validation

This section will discuss the comparison of the results of the numerical model produced by X-beach and the results of field data recorded through two types of recording devices that have been installed in the field, namely the Water level meter and the current speed meter (ADCP), initial modeling effort was done using default X-beach setting and recorded data at Mentayan Beach on May 22, 2019, for 24 hours, the purpose of this activity is to verify the suitability of the default setting.

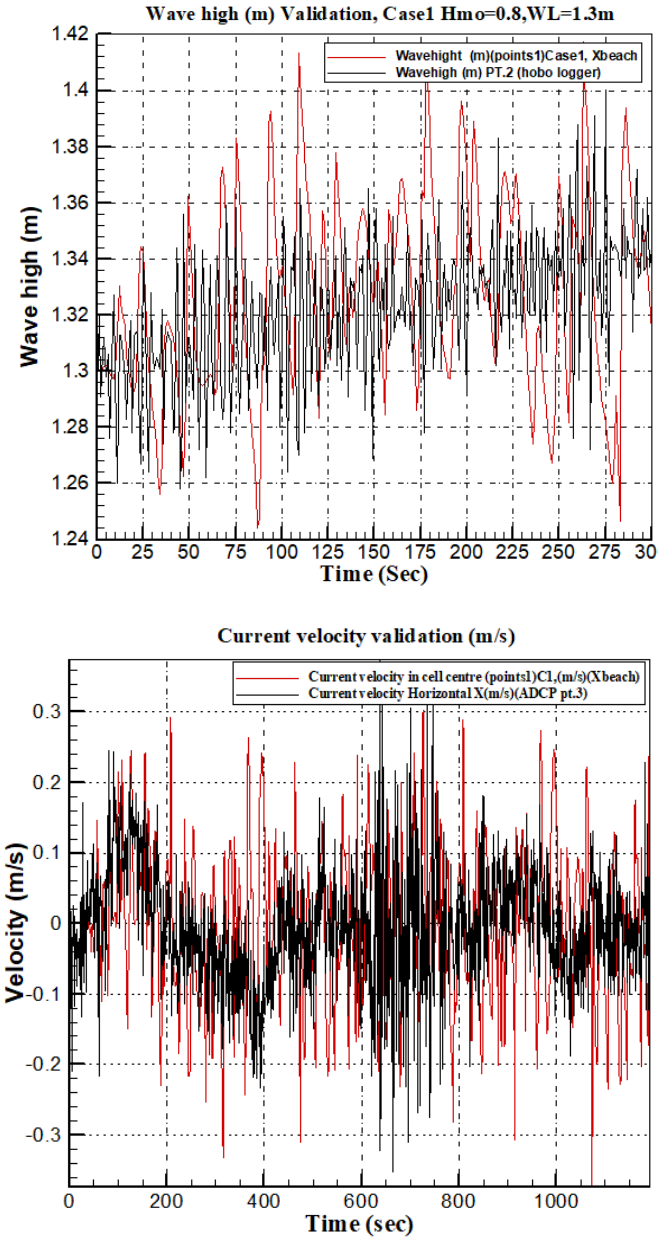

Fig. 11. Result of the validation run with default X beach model setting and Field data observation, wave high validation, black lines indicated wave high recorded by hobo logger pt.2 and red lines indicated Xbeach model(upper), Current velocity validation, black lines indicated current velocity recorded by ADCP pt.3, red lines indicated Xbeach model (lower)

The positive results of this validation model can be seen from the ability of xbeach to simulate wave heights and speed of currents, this can be seen in the figure.8, the solid black line is the data obtained from observations in the field while the solid red line is the result of xbeach

simulation. The model parameter settings on xbeach are made in such a way that they are close to the actual conditions in accordance with the study area, to understand the ability of the three types of mangroves in an effort to reduce the erosion rate at Bengkalis Island Six case were selected for each type of mangrove. For information on each case can be seen in Table 2.

3. Result and Discussion

The eroded part is defined as the lower area of the initial profile and the creation as the part that is above the initial profile, to determine the amount of erosion volume can be calculated by comparing the cliff volume below the initial profile at the start with the cliff volume below the profile measured, erosion and creations that occur can be modeled as dynamic behavior as a consequence of external forces from waves and currents.

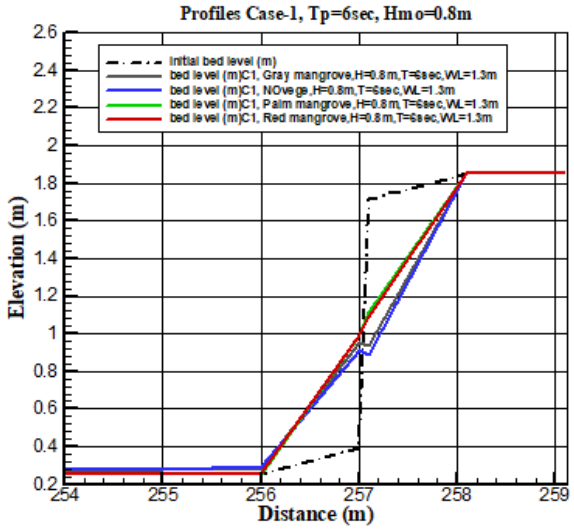

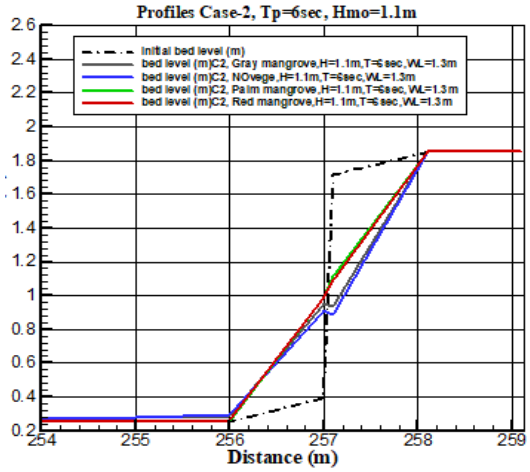

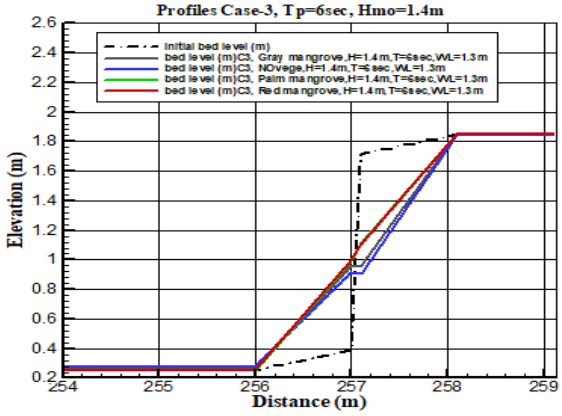
Profiles Case-3, Tp=6sec, Hmo=1.4m
Initial bed level (m)
bed level (m)C3, Gray mangrove,H=1.4m,T=6sec,WL=1.3m
bed level (m)C3, NOvege,H=1.4m,T=6sec,WL=1.3m
bed level (m)C3, Palm mangrove,H=1.4m,T=6sec,WL=1.3m
bed level (m)C3, Red mangrove,H=1.4m,T=6sec,WL=1.3m
Elevation (m)
Distance (m)

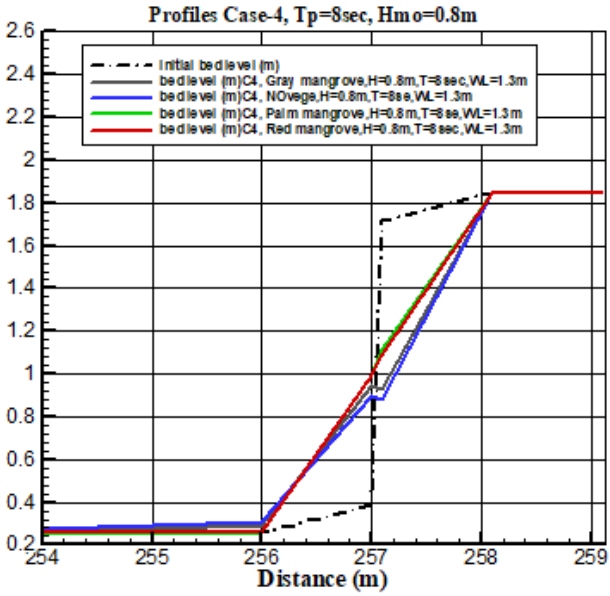
Profiles Case-4, Tp=8sec, Hmo=0.8m
Initial bed level (m)
bed level (m)C4, Gray mangrove,H=0.8m,T=8sec,WL=1.3m
bed level (m)C4, NOvege,H=0.8m,T=8se,WL=1.3m
bed level (m)C4, Palm mangrove,H=0.8m,T=8se,WL=1.3m
bed level (m)C4, Red mangrove,H=0.8m,T=8sec,WL=1.3m
Distance (m)

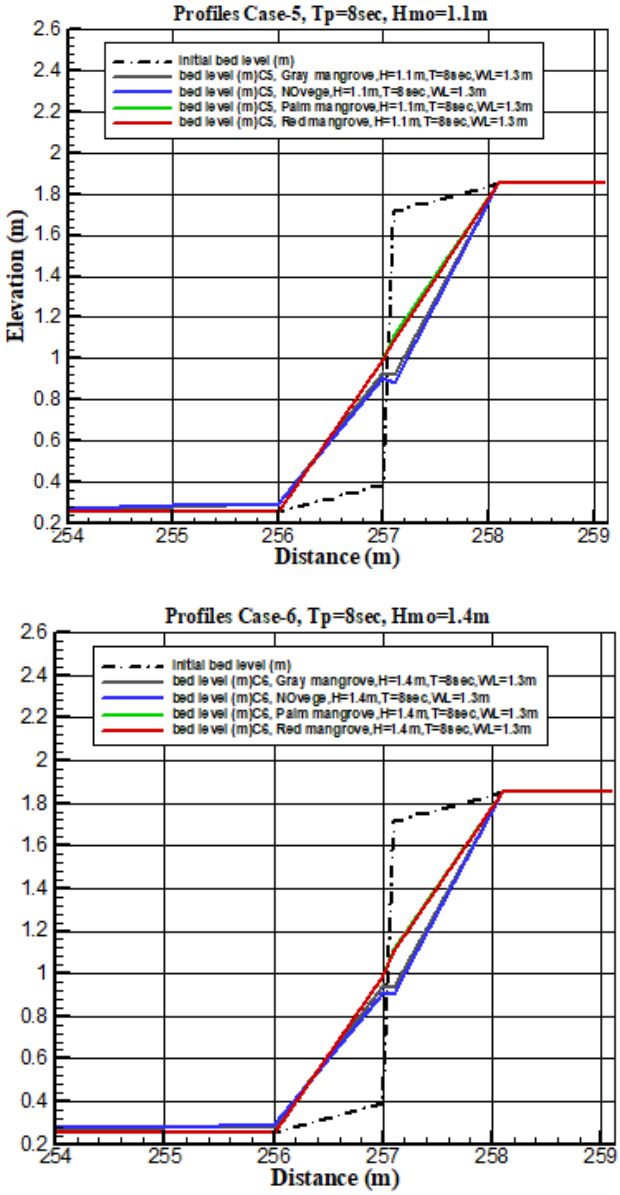

Fig. 12. Erosion profile on the cliff for all different cases, Upper left panel case 1, upper right panel case 2, middle left panel case 3, middle right panel case 4, lower left panel case 5 and lower right panel case 6

From the Figure 12, it can be seen that the mangrove tree with the type of palm mangrove indicates as solid green line has the greatest ability in reducing of erosion. The area of wave propagation or wave breaking in an additional dissipation mechanism for short wave. The short wave dissipation due to vegetation is calculated as function of the local wave height and vegetation parameter.

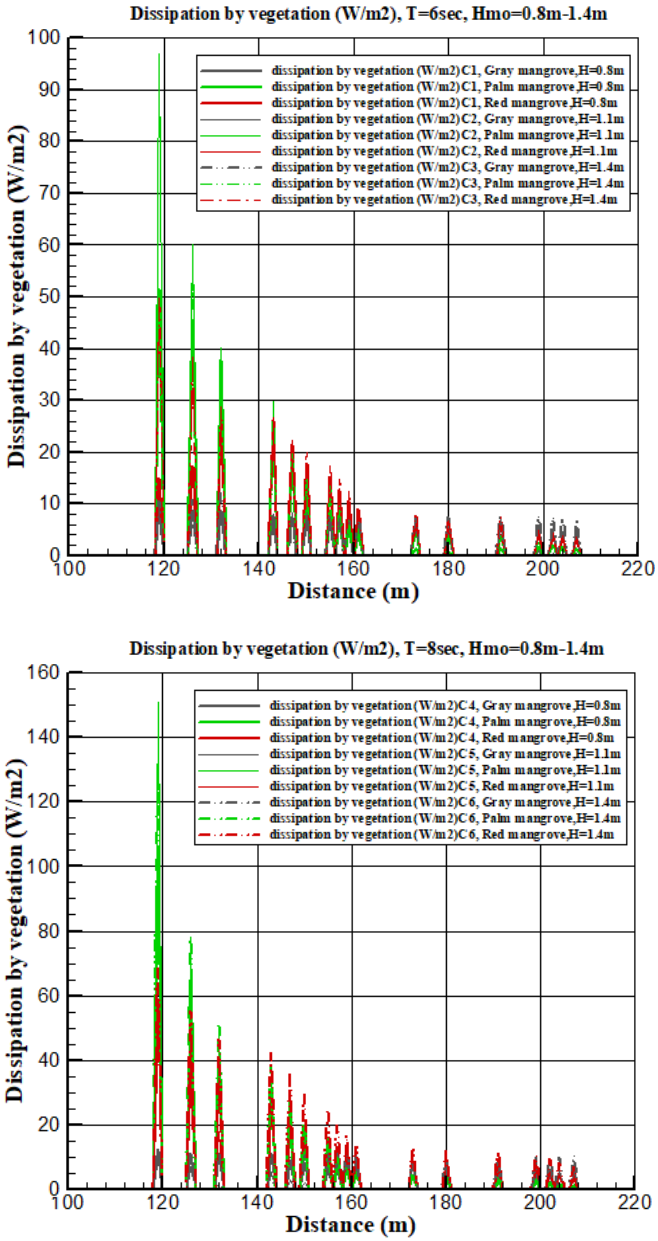

Fig. 13. Variation in Hmo for Dissipation due to shortwave attenuation by vegetation, for T=6 sec (upper) for T=8sec (lower)

Palm mangrove has a greater ability in this regard can be seen from the picture above which is marked with a green line for palm mangrove, gray line for mangrove gray and red line for red mangrove, dissipation has a greater value when short waves begin to enter the mangrove area and seen decreasing when heading to the coast, from the two graphs above also shows that the greater the value of the wave period, the greater the value of dissipation by vegetation.

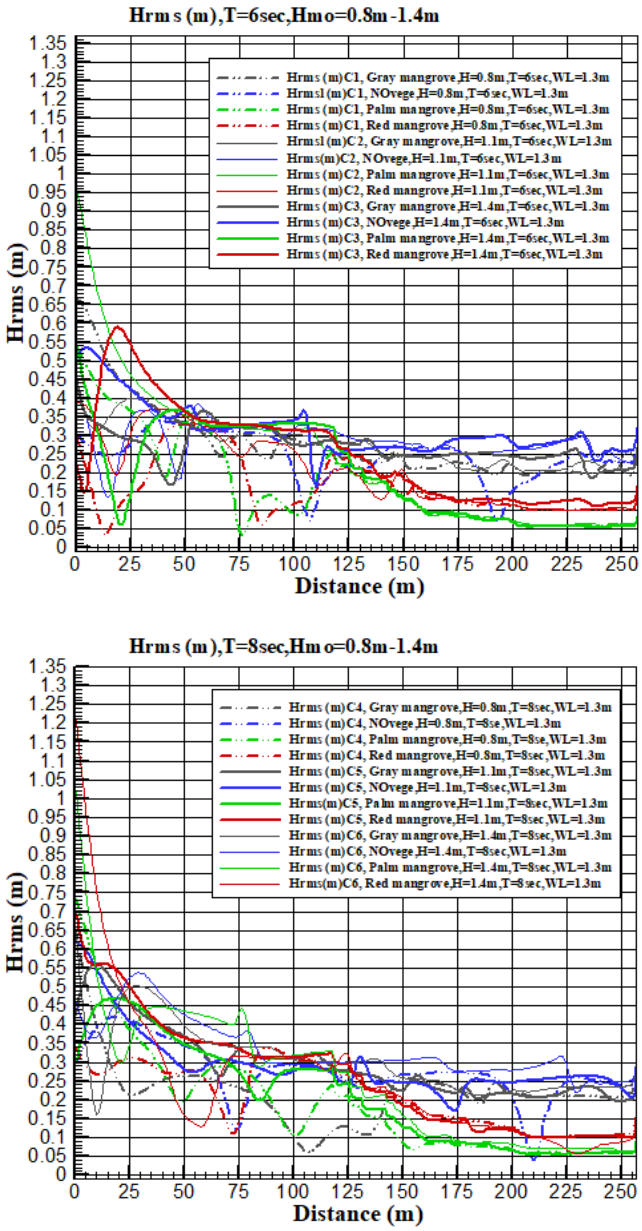

Fig. 14. Hrms in Hmo Variation for every cases, for Wave priode (T)= 6 second (upper), T=8second (lower)

For the case with vegetation, it can be noticed that wave propagation without obstruction to the beach cliff, from the figure we can calculate the wave reduction factor, defined as:

$$r = \frac{\Delta H}{H.\Delta x} \tag{16}$$

Where Δ H is the difference in wave height between initial wave height and the wave height at the end of mangrove forest transect. Δx defined as the distance for the mangrove in this study 95 m. The r value for each case will be displayed in the following table

Table 5. R value for every case

Case	Mangrove Type	T (sec)	Hmo (m)	R (m^{-1})
	Gray Mangrove	6	0.8	0.002688
1	Palm mangrove	6	0.8	0.008103
	Red mangrove	6	0.8	0.00583
	Gray Mangrove	6	1.1	0.003093
2	Palm mangrove	6	1.1	0.008095
	Red mangrove	6	1.1	0.004664
	Gray Mangrove	6	1.4	0.001787
3	Palm mangrove	6	1.4	0.008706
	Red mangrove	6	1.4	0.006596
	Gray Mangrove	8	0.8	0.001875
4	Palm mangrove	8	0.8	0.00777
	Red mangrove	8	0.8	0.006922
	Gray Mangrove	8	1.1	0.003251
5	Palm mangrove	8	1.1	0.008518
	Red mangrove	8	1.1	0.007211
	Gray Mangrove	8	1.4	0.002719
6	Palm mangrove	8	1.4	0.008238
	Red mangrove	8	1.4	0.006664

From the Table 5, it can be seen that the highest value of wave reduction factor (R) is shown by the mangrove palm and the lowest by gray mangrove, for cases with a wave period of 6 seconds the maximum R value for palm mangrove is 0.0081-0.0087 m^{-1}, for wave period 8 seconds the r value for palm mangrove is 0.0077 - 0.0085 m^{-1}, the lowest r value for gray mangrove is 0.0017 - 0.003 m^{-1} for wave period 6 seconds and 0.0018 - 0.0032 m^{-1}.

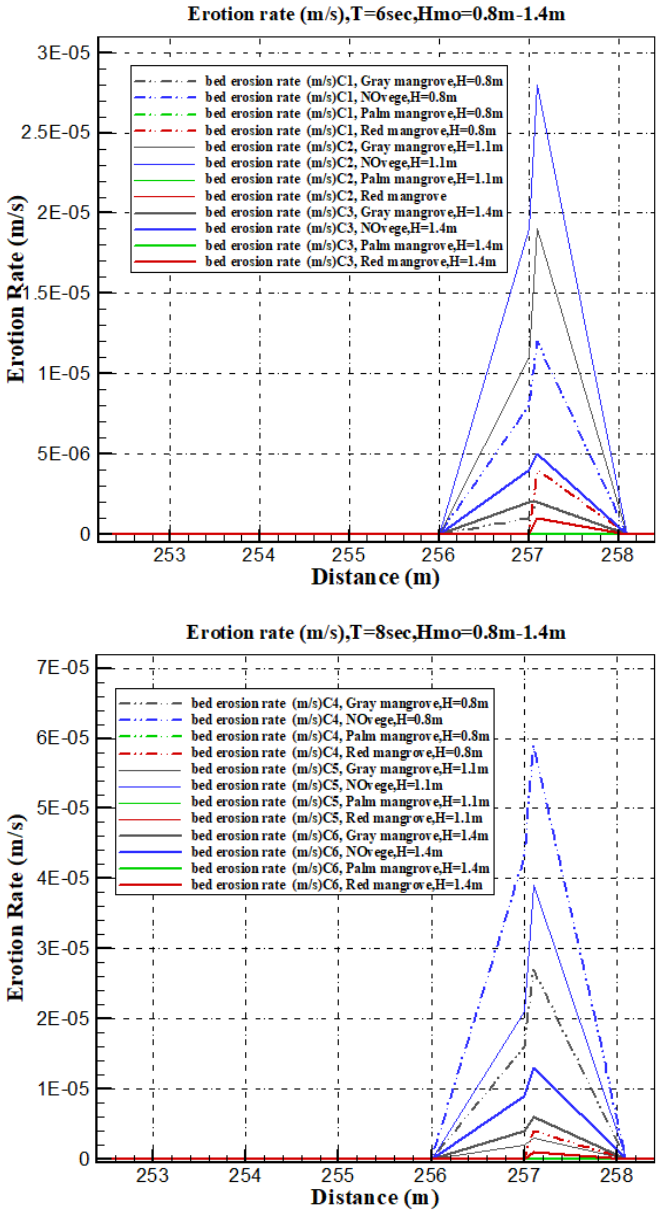

Fig. 15. Erosion rate (m/s) in Hmo Variation for every cases, for Wave period T = 6 second (upper), T = 8 second (lower)

The erosion rate measures the amount of soil mass lost over a specified time of wave period. The x-beach model that occurs in toppling failure is a function of the eroded region width and wave period, this can be seen from the total number of eroded deposits near the shoreline, the greater the wave period the erosion rate will be greater. The most rate erosion rate occurs for the condition with wave period T = 6s and high h_{mo} = 1.1 m, at this condition the water level is on a stem layer that has a low Dveg value, gray mangrove species marked with a thin gray line

have the ability to the lowest in holding the speed of erosion rate, followed by the type of red mangrove. of the three types of mangroves compared, palm mangrove see Figure 7 can withstand the erosion rate.
nology implementation on the MSME community in Bengkalis.

4. Conclusion

This research aims to study the erosion process and the ability of all three types of mangroves in reducing the erosion rate at Bengkalis island from a numerical approach. All of the mangrove tree samples taken in this study are located on the Mentayan beach located on the north side of the Bengkalis Island. X-beach 1D model simulates the wave attenuation in the mangrove tree, and calculate the vegetation effect to reduce the erosion rate. The simulation result shows that the mangrove palm, although only defined has two layers, namely the stem and canopy but overall have a better ability to reduce the erosion rate. From the three types of mangroves compared in this study, the type of the gray mangrove has the weakest capability of the others, although this type of mangrove is a type that is recommended by local governments as a type of mangrove to be planted in offshore areas because of its superiority, namely have fast growth, but during our field observations, we found that there are many dead plants of this species, so it can be concluded that this species is not a good type to plant near the offshore side. What better choice on the type of mangrove red mangrove and palm mangrove, further research is needed to examine the ability of mangroves to store the sediment from eroded materials

Nomenclature

a	specific surface area	m^2m^{-3}
x	length co-ordinate	m
Greek letters		
α	heat transfer coefficient	$Wm^{-2}K^{-1}$
τ	residence time	s
Subscripts		
i	inlet	
e	equilibrium	

Acknowledgements

This work was supported by Indonesia Endowment Fund for Education (LPDP), Ujigawa Hydraulics Laboratory DPRI Kyoto University.

References

[1] S. M. Metev and V. P. Veiko, *Laser Assisted Microtechnology*, 2nd ed., R. M. Osgood, Jr., Ed. Berlin, Germany: Springer-Verlag, 1998.

[2] J. Breckling, Ed., *The Analysis of Directional Time Series: Applications to Wind Speed and Direction*, ser. Lecture Notes in Statistics. Berlin, Germany: Springer, 1989, vol. 61.
[3] S. Zhang, C. Zhu, J. K. O. Sin, and P. K. T. Mok, "A novel ultrathin elevated channel low-temperature poly-Si TFT," *IEEE Electron Device Lett.*, vol. 20, pp. 569–571, Nov. 1999.
[4] M. Wegmuller, J. P. von der Weid, P. Oberson, and N. Gisin, "High resolution fiber distributed measurements with coherent OFDR," in *Proc. ECOC'00*, 2000, paper 11.3.4, p. 109.
[5] R. E. Sorace, V. S. Reinhardt, and S. A. Vaughn, "High-speed digital-to-RF converter," U.S. Patent 5 668 842, Sept. 16, 1997.
[6] (2002) The IEEE website. [Online]. Available: http://www.ieee.org/
[7] M. Shell. (2002) IEEEtran homepage on CTAN. [Online]. Available: http://www.ctan.org/tex-archive/macros/latex/contrib/supported/IEEEtran/
[8] *FLEXChip Signal Processor (MC68175/D)*, Motorola, 1996.
[9] "PDCA12-70 data sheet," Opto Speed SA, Mezzovico, Switzerland.
[10] A. Karnik, "Performance of TCP congestion control with rate feedback: TCP/ABR and rate adaptive TCP/IP," M. Eng. thesis, Indian Institute of Science, Bangalore, India, Jan. 1999.
[11] J. Padhye, V. Firoiu, and D. Towsley, "A stochastic model of TCP Reno congestion avoidance and control," Univ. of Massachusetts, Amherst, MA, CMPSCI Tech. Rep. 99-02, 1999.
[12] *Wireless LAN Medium Access Control (MAC) and Physical Layer (PHY) Specification*, IEEE Std. 802.11, 1997.
[13] Allen, J.R.L. (1989). Evolution of salt-marsh cliffs in muddy and sandy systems: a qualitative comparison of British west-coast estuaries. Earth Surface Pro- cesses and Landforms 14 (1), pp. 85–92.
[14] Bendoni Michele (2016). Salt marsh edge erosion due to wind-induced waves. Dissetation book, Department of Architecture, Civil Engineering and Environmental Sciences. University of Braunschweig – Institute of Technology
[15] Flemming, B.W. (2000). A revised textural classification of gravel-free muddy sediments on the basis of ternary diagrams. Continental Shelf Research 20 (10), pp. 1125–1137.
[16] Francalanci, S., M. Bendoni, M. Rinaldi, and L. Solari (2013). Ecomorphody- namic evolution of salt marshes: Experimental observations of bank retreat processes. Geomorphology 195, pp. 53–65.
[17] Jacobs, W., P. Le Hir, W. Van Kesteren, and P. Cann (2011). Erosion threshold of sand–mud mixtures. Continental Shelf Research 31 (10), S14–S25.
[18] Oumeraci, H. and A. Kortenhaus (1994). Analysis of the dynamic response of caissons breakwaters. Coastal Engineering 22, pp. 159–183.
[19] Rijn, L. C. V. (1993). Principles of sediment transport in rivers, Estuaries and coastal seas. Aqua Publication.
[20] Robert McCall, N. P., Jaap van Thiel de Vries (2010). "The effect of longshore topographic variation on Overwash modelling." Coastal Engineering.
[21] Roelvink. J. A., A. J. H. M. R., A. R. van Dongeren, J. S. M. van Thiel de Vries, R. T. McCall, and Jamie Lescinski (2009). "Modelling storm impacts on beaches, dunes and barrier islands." Coastal Engineering 56: 1133–1152.
[22] Roelvink J. A., M. J. F. S. (1998). "Bar-generating cross-shore flow mechanisms on a beach." Journal of Geophysical Research 94: 4785–4800.
[23] Ruessink B. G., G. R., and L. C. van Rijn (2012). "On the parameterization of the free-stream non-linear wave orbital motion in nearshore morpho-dynamic models." Coastal Engineering 65: 56–63.

[24] Ruessink B. G., J. R. M., F. Feddersen, R. T. Guza, and Steve Elgar (2001). "Modeling the alongshore current on barred beaches." Journal of Geophysical Research 106(22): 451–463.
[25] Service, U. S. A. (1955). Bengkalis Map, Series T503. Sheet Number NA48-49.
[26] Teams of Xbeach. (2017). Xbeach Documentation Release pre-1.22.4344.
[27] Theerawitaya, C, Samphumphaung,T, Cha-um, S Nana Yamada, N. and Takabe, T. 2014. Responses of Nipa palm (Nypa fruticans) seedlings, a mangrove species, to salt stress in pot culture. Flora - Morphology, Distribution and Functional Ecology of Plants 209 (10):597-603
[28] Thorne, C.R. and N.K. Tovey (1981). Stability of composite river banks. Earth Surface Processes and Landforms 6 (5), pp. 469–484.
[29] Van Rijn, L.C. (1993). Principles of Sediment Transport in Rivers, Estuaries and Coastal Seas. Vol. 2. 3. Aqua publications Amsterdam.